catalysts

MDPI

Article

Promoting Effect of Mn on In Situ Synthesized Cu-SSZ-13 for NH_3-SCR

Jinpeng Du [1,2,†], Jingyi Wang [2,3,†], Xiaoyan Shi [1,2], Yulong Shan [1], Yan Zhang [3] and Hong He [1,2,3,*]

1 State Key Joint Laboratory of Environment Simulation and Pollution Control, Research Center for Eco-Environmental Sciences, Chinese Academy of Sciences, Beijing 100085, China; jpdu_st@rcees.ac.cn (J.D.); xyshi@rcees.ac.cn (X.S.); ylshan@rcees.ac.cn (Y.S.)
2 University of Chinese Academy of Sciences, Beijing 100049, China; jywang1@iue.ac.cn
3 Center for Excellence in Regional Atmospheric Environment, Institute of Urban Environment, Chinese Academy of Sciences, Xiamen 361021, China; yzhang3@iue.ac.cn
* Correspondence: honghe@rcees.ac.cn; Tel.: +86-010-6284-9123
† Jinpeng Du and Jingyi Wang contributed equally to this work.

Received: 23 October 2020; Accepted: 23 November 2020; Published: 25 November 2020

Abstract: The effect of Mn impregnation on the NH_3-SCR (selective catalytic reduction of NO_x by NH_3) activity of in situ synthesized Cu-SSZ-13 was investigated in this work. It was found that Mn addition could efficiently improve the low-temperature activity of Cu-SSZ-13. The optimal amount of Mn was 5 wt.%, and NO_x conversion was improved by more than 20% over a temperature range of 120 °C to 150 °C. SEM (scanning electron microscopy), XRD (X-ray diffraction), N_2 adsorption-desorption, H_2-TPR (temperature programmed reduction of H_2), NH_3-TPD (temperature programmed desorption of NH_3) and in situ DRIFTS (diffuse reflectance infrared Fourier transform spectroscopy) experiments were conducted to investigate the changes in the zeolite structure, active sites, acid sites and reaction mechanism. The impregnated MnO_x species caused a decline in the crystallinity of Cu-SSZ-13 but markedly improved the redox ability. Nitrate and nitrite species were observed in the Mn-modified Cu-SSZ-13, and the formation of these species was thought to cause the observed increase in low-temperature NH_3-SCR activity. The results show that the addition of Mn is a promising method for promoting the low-temperature catalytic activity of Cu-SSZ-13.

Keywords: NH_3-SCR; in situ synthesized Cu-SSZ-13; Mn impregnation; low-temperature catalytic activity

1. Introduction

The emission of nitrogen oxides (NO_x) from heavy-duty diesel vehicles makes a large contribution to atmospheric pollution [1–3]. The selective catalytic reduction of NO_x by NH_3 (NH_3-SCR) has proven to be one of the most efficient technologies for NO_x abatement from heavy-duty diesel vehicles [4–8]. As an NH_3-SCR catalyst, Cu-SSZ-13 zeolite has, with its small-pore structure, attracted much attention in recent years [9–11]. NH_3-solvated Cu ions, which are weakly tethered to framework Al and regarded as mobile active sites, make the NH_3-SCR reaction occur in a near-homogeneous fashion in a limited region [12]. The pore size of Cu-SSZ-13 is around 3.8 Å, which screens large molecules such as HCs from entering the zeolite cavities and also restricts the out-diffusion of $Al(OH)_3$ species formed under hydrothermal conditions [13]. Therefore, the special pore structure endows Cu-SSZ-13 with excellent NH_3-SCR activity, N_2 selectivity, HCs resistance and hydrothermal stability.

Ren et al. invented an in situ synthesis method for Cu-SSZ-13 that uses Cu-tetraethylenepentamine (Cu-TEPA) as a template to directly introduce Cu into the precursor gel [14,15]. Compared with the conventional ion-exchange method, this in situ synthesis method avoids the complicated ion-exchange

process and reduces the production of wastewater, which is beneficial for practical application. Furthermore, Xie et al. and Shan et al. optimized the structure of and copper species in in situ synthesized Cu-SSZ-13 by HNO_3 and NH_4NO_3 after treatment, leading to marked increases in the catalytic activity and hydrothermal stability [16,17]. Nevertheless, the low-temperature activity (<180 °C) of in situ synthesized Cu-SSZ-13 is still low and needs to be improved [18–20].

Numerous studies showed that, at temperatures below 180 °C, Mn-based catalysts were very active in the NH_3-SCR reaction [21–27]. For instance, over 90% NO_x conversion could be obtained over MnO_x-CeO_2 complex oxide catalysts at 150 °C [21,28]. Tang et al. doped a series of metals on Mn-based catalysts, and they found that the Mn-Fe-Ce catalyst performed the best. A 95% NO_x conversion could be obtained, and it also had an excellent SO_2 and H_2O tolerance [27]. Ye et al. synthesized a series of Mn/SSZ-13 catalysts with various Mn loadings, and over 95% NO_x conversion was obtained at 150 °C for the best sample [29]. Meanwhile, Mn-based bimetallic zeolites also showed excellent low-temperature NH_3-SCR activity. Kim et al. added Mn into the Fe-ZSM-5 catalyst, and the catalytic performance was improved [30]. The NO_x conversion of Cu-SSZ-39 was also raised over the whole temperature range after the addition of Mn [31]. Song et al. synthesized Cu-Mn-SSZ-13 catalysts by a coexchange method, and both the catalytic activity and hydrothermal stability were improved with the appropriate loading amount [32]. It seems that the addition of Mn has positive effects on the NH_3-SCR activity of Cu-SSZ-13. To meet the demands of a practical application, the low-temperature catalytic activity of in situ synthesized Cu-SSZ-13, which is one of the most promising catalysts utilized in heavy-duty diesel vehicles, should also be of concern.

In this study, a series of Mn/Cu-SSZ-13 catalysts with various Mn loadings were prepared by impregnating manganese acetates into in situ synthesized Cu-SSZ-13. The results showed that the addition of Mn could improve the catalytic performance of Cu-SSZ-13 catalysts. The effects of Mn impregnation on the zeolite framework and morphology of Cu-SSZ-13 were characterized by XRD and SEM. H_2-TPR and NH_3-TPD were utilized to assess the redox ability and acidity of Cu-SSZ-13 and Mn/Cu-SSZ-13. In addition, a series of in situ DRIFTS experiments were carried out to investigate the NH_3-SCR mechanism over the prepared catalysts.

2. Results and Discussion

2.1. NH_3-SCR Performance

The standard NH_3-SCR catalytic activity profiles of all the prepared catalysts are presented in Figure 1. As can be seen, all the catalysts showed a broad window of over 90% NO_x conversion from around 160 °C to 330 °C. As can be seen, after impregnation with Mn, all catalysts presented a better catalytic activity below 160 °C when compared with Cu-SSZ-13. Among all the catalysts, 5% Mn/Cu-SSZ-13 showed the best catalytic activity in the low temperature range, and nearly 95% NO_x conversion was obtained around 140 °C. With a further increase in the Mn content, however, the low-temperature NO_x conversion began to decrease when compared with 5% Mn/Cu-SSZ-13. To analyze the selectivity of the prepared catalysts, the N_2O concentrations in the effluents from the catalysts are summarized in Figure S1. More N_2O was produced with an increase of the Mn content, indicating that the addition of Mn would decrease the N_2 selectivity of the catalysts. Nevertheless, the N_2O formation was under 20 ppm for Mn/Cu-SSZ-13 with an Mn content below 7%. The accurate control of the Mn content was of vital importance to the catalytic performance, and 5% Mn/Cu-SSZ-13 performed the best among all the prepared catalysts. The following sections will compare the characterization results between 5% Mn/Cu-SSZ-13 and Cu-SSZ-13; the promotion effect of Mn on Cu-SSZ-13 was also investigated.

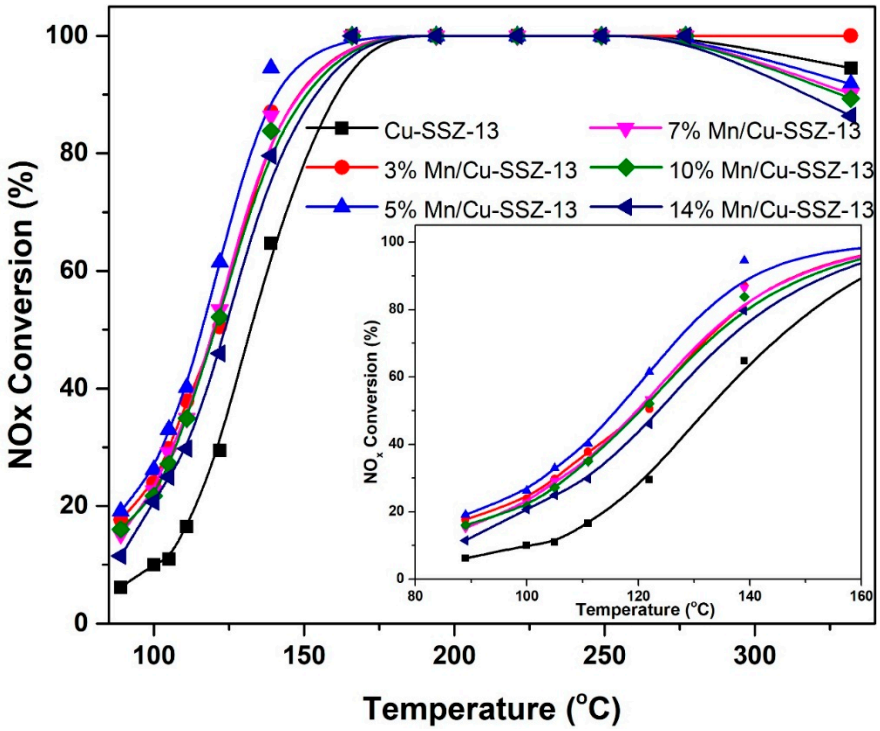

Figure 1. NH_3-SCR performance of the prepared catalysts. Test conditions: [NO] = [NH_3] = 500 ppm, [O_2] = 5%, N_2 balance, GHSV = 100,000 h^{-1}.

2.2. Characterization of Catalysts

The SEM images illustrate the morphology of Cu-SSZ-13 (Figure 2a) and 5% Mn/Cu-SSZ-13 (Figure 2b). As can be seen, in both cases the catalyst grains had a cubic shape with a crystallite size of around 300–500 nm. No discernable destruction of the grains could be observed after 5% Mn was impregnated into Cu-SSZ-13, indicating that the morphology of Cu-SSZ-13 was not affected by doping with Mn. Furthermore, the N_2 adsorption-desorption experimental results showed that the surface area and pore volume were 613 m^2/g and 0.212 cm^3/g for Cu-SSZ-13, and 596 m^2/g and 0.206 cm^3/g for 5% Mn/Cu-SSZ-13. Compared with Cu-SSZ-13, there was only a slight decrease in the surface area and pore volume for 5% Mn/Cu-SSZ-13, indicating that the channel structure was not affected by Mn impregnation. In addition, the SEM images of catalysts with other Mn contents are presented in Figure S2. The morphologies of these catalysts showed little change after Mn impregnation, except for 14% Mn/Cu-SSZ-13, which showed some degradation of the structure. In summary, when the Mn content was below 10%, the MnO_x species over Cu-SSZ-13 were highly dispersed and did not affect the channel structure of Cu-SSZ-13.

Furthermore, EDX was utilized to detect the composition of atoms in Cu-SSZ-13 and 5% Cu-SSZ-13, and the results are presented in Figure S3. Ten spots were scanned for each catalyst, and the atomic composition was calculated as the average value of the 10 spots. As can be seen, there were fewer O, Al, Si and Cu atoms in 5% Mn/Cu-SSZ-13 than in Cu-SSZ-13, which was due to the addition of Mn. Meanwhile, EDS could only detect the atoms on the surface of the catalysts. 5% Mn was added into the catalysts; however, only 1.8% Mn was detected. These results indicated that more Mn atoms were located in the pores of Cu-SSZ-13, which was in accordance with the results of the SEM images.

The XRD patterns of Cu-SSZ-13 and 5% Mn/Cu-SSZ-13 are presented in Figure 3. Both catalysts showed the typical diffraction peaks of the CHA structure, indicating that the addition of Mn did not change the zeolite structure of CHA. Meanwhile, no peaks resulting from CuO_x species could be observed for either Cu-SSZ-13 or 5% Mn/Cu-SSZ-13. Compared with Cu-SSZ-13, no new diffraction peaks emerged in the pattern of 5% Mn/Cu-SSZ-13, which meant that the MnO_x species were highly dispersed. This result was in accordance with the SEM images, which showed no evidence of MnO_x

species accumulation. The XRD patterns of all the prepared catalysts are presented in Figure S4. With the increase in the Mn content, the crystallinity of the catalysts decreased, which meant that Mn impregnation could lead to the deterioration of the framework of Cu-SSZ-13.

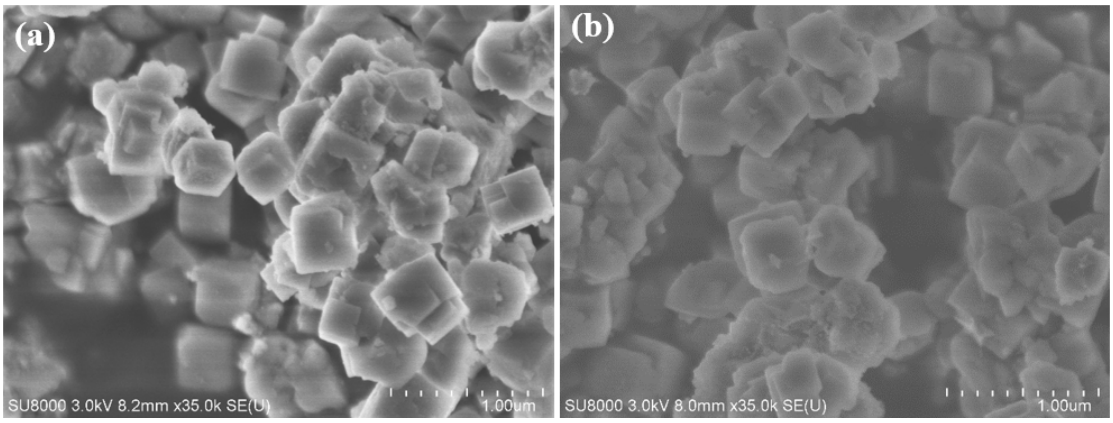

Figure 2. SEM images of (**a**) Cu-SSZ-13 and (**b**) 5% Mn/Cu-SSZ-13.

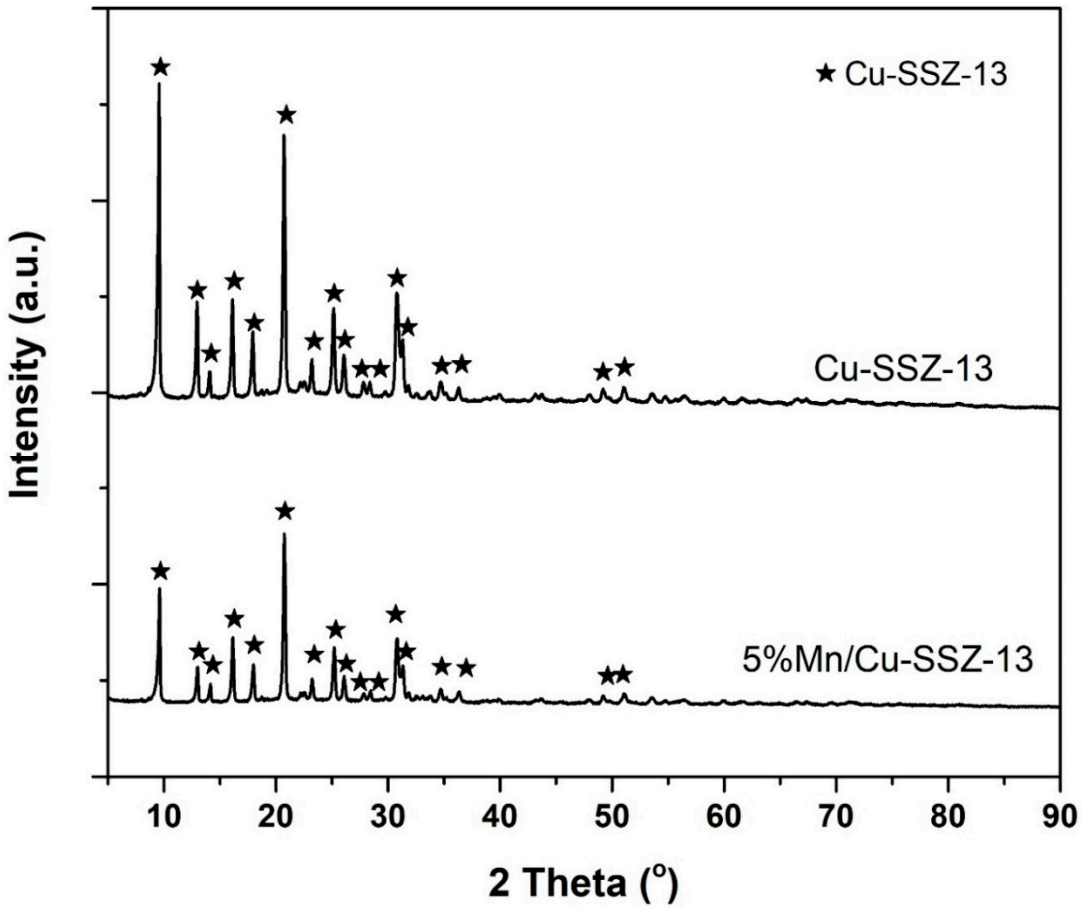

Figure 3. XRD patterns of Cu-SSZ-13 and 5% Mn/Cu-SSZ-13.

H_2-TPR experiments were carried out to evaluate the redox ability of the catalysts, and the results are presented in Figure 4. Three peaks can be observed under 500 °C for Cu-SSZ-13. Peak A was assigned to the reduction of $Cu(OH)^+$ species in CHA cages; peak B was attributed to the reduction of CuO_x species; and peak C represented the consumption of H_2 by Cu^{2+} species near d6r [33,34]. It is

worth mentioning that no peak corresponding to CuO_x species was observed in the XRD patterns, indicating that these CuO_x species were highly dispersed. In the H_2-TPR curve of 5% Mn/Cu-SSZ-13, five peaks can be observed. The reduction of $Cu(OH)^+$ species in CHA cages, CuO_x species and Cu^{2+} species near d6r were also included in Peaks A, B and C [16,33,35–37]. However, the peaks for the Cu species shifted to a lower temperature, indicating that the redox ability was improved. Compared to Cu-SSZ-13, there was an increase in the areas of peak A and B, and a decrease in the area of peak C. The decline of peak C can be attributed to a decrement in the amount of Cu^{2+} species near d6r, because the impregnated Mn ions might occupy some ion-exchange sites. Meanwhile, the increase in peak B was partially due to the formation of new CuO species, which emerged because the ion-exchange sites of Cu ions were occupied by Mn ions. During the addition of Mn, $Cu(OH)^+$ species in CHA cages must have been lost, since these species are less stable than Cu^{2+} species near d6r. However, the area of peak A increased, which meant that MnO_x species also contributed to peak A. Furthermore, peak D and peak E also emerged as new peaks after the Mn addition, and they were also assigned to the reduction of MnO_x species. In the previous literature, the reduction peaks of pure MnO_x oxides by H_2 were frequently observed in the range between 300 °C and 600 °C, and the reduction of these species occurred by a three-step process: $MnO_2 \rightarrow Mn_2O_3 \rightarrow Mn_3O_4 \rightarrow MnO$ [38,39]. However, with the addition of other elements, the H_2-TPR peaks of MnO_x species could move to much lower temperatures [40,41]. Therefore, in this study, the reduction of MnO_2 to Mn_2O_3 occurred in the range of 150 °C to 350 °C; peak D represented the reduction of Mn_2O_3 to Mn_3O_4, and peak E was assigned to the reduction of Mn_3O_4 to MnO. Impregnation with Mn efficiently improved the redox ability of Cu-SSZ-13. The reaction process of NH_3-SCR over Cu-SSZ-13 was accompanied with an electron transfer between Cu ions and the reactants [9,12,42]. A better redox ability for catalysts might facilitate the electron transfer process, resulting in an improvement in the catalytic activity. As a result, the better redox ability of 5% Mn/Cu-SSZ-13 could be one of the reasons why it exhibited a higher low-temperature activity than Cu-SSZ-13.

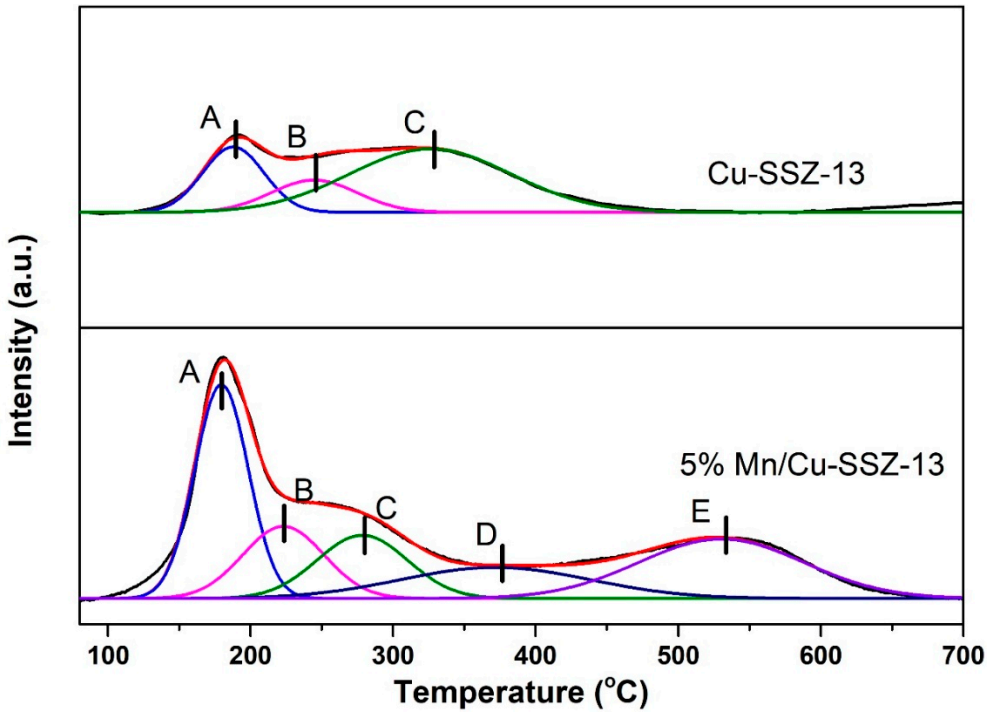

Figure 4. H_2-TPR curves of Cu-SSZ-13 and 5% Mn/Cu-SSZ-13.

XPS was utilized to detect the oxidation state of Cu in Cu-SSZ-13 and Cu & Mn in 5% Mn/Cu-SSZ-13. As presented in Figure S5a, the binding energy values of Cu 2p 1/2 and Cu 2p 3/2 were 953.9 eV and 934.0 eV in both catalysts, respectively. Meanwhile, there were satellite peaks around 965~962 eV and

941~949 eV in 5% Mn/Cu-SSZ-13; however, no satellite peaks were observed in Cu-SSZ-13 [26,27]. Through the deconvolution of the peak with a binding energy of around 940~930 eV, the composition of Cu ions with different valence states was calculated. 75.2% of Cu ions in Cu-SSZ-13 consisted of Cu^{2+}, compared with 86.8% Cu^{2+} in 5% Mn/Cu-SSZ-13. A higher amount of Cu^{2+} was beneficial for a low-temperature catalytic activity, so that 5% Mn/Cu-SSZ-13 performed better [26]. Furthermore, the Mn 2p spectra of 5% Mn/Cu-SSZ-13 are presented in Figure S5b, and the binding energy values at 655.3 eV and 643.2 eV were assigned to Mn 2p 1/2 and Mn 2p 3/2, respectively [26,27,39]. To calculate the composition of Mn ions, the peak around 650~640 eV was deconvoluted; the contents of Mn^{2+}, Mn^{3+} and Mn^{4+} ions were 17.9%, 62.3% and 19.8%, respectively. As a result, in addition to there being more Cu^{2+} ions in 5% Mn/Cu-SSZ-13, another reason why Mn-impregnated catalysts performed better in the low-temperature range was the presence of a large amount of Mn^{3+} and Mn^{4+} ions [26,27,39].

To compare the acidity of Cu-SSZ-13 and 5% Mn/Cu-SSZ-13, NH_3-TPD experiments were carried out, and the results are shown in Figure 5. After the deconvolution of the NH_3 desorption profiles, three peaks could be observed for both catalysts. According to the desorption temperature of NH_3, Peak A, Peak B and Peak C were assigned to the desorption of NH_3 from weak acid sites, medium acid sites and strong acid sites, respectively. To further analyze the amount of each kind of acid site, the NH_3 desorption amount per 1 g of catalyst was calculated, and the results are presented in Figure S6. Overall, 5% Mn/Cu-SSZ-13 possessed more acid sites than Cu-SSZ-13, which was attributed to the contribution of the MnO_x species. For Cu-SSZ-13, the weakly adsorbed NH_3 could be attributed to surface hydroxyl species; the medium acid sites were assigned to Lewis acid sites, which were mainly from Cu^{2+} species; and the strong acid sites originated from Brønsted acid sites [43–45]. Meanwhile, the desorption of NH_3 from MnO_x species could be observed in the range of 100 °C to 500 °C, so that MnO_x species in 5% Mn/Cu-SSZ-13 contributed to weak, medium and strong acid sites simultaneously [46–48]. The amount of weakly absorbed NH_3 that was desorbed was 0.82 mmol/g for 5% Mn/Cu-SSZ-13, while it was 0.55 mmol/g for Cu-SSZ-13. Meanwhile, the amount of NH_3 that was desorbed from strong acid sites was 0.59 mmol/g and 0.44 mmol/g for 5% Mn/Cu-SSZ-13 and Cu-SSZ-13, respectively. However, it is worth mentioning that Cu-SSZ-13 possessed more medium acid sites than 5% Mn/Cu-SSZ-13. This could be due to Cu-SSZ-13 possessing more Cu^{2+} species than 5% Mn/Cu-SSZ-13, which was in accordance with the H_2-TPR results. In conclusion, the increase in the numbers of weak and strong acid sites after the addition of Mn could also be one of the reasons why catalytic activity was promoted.

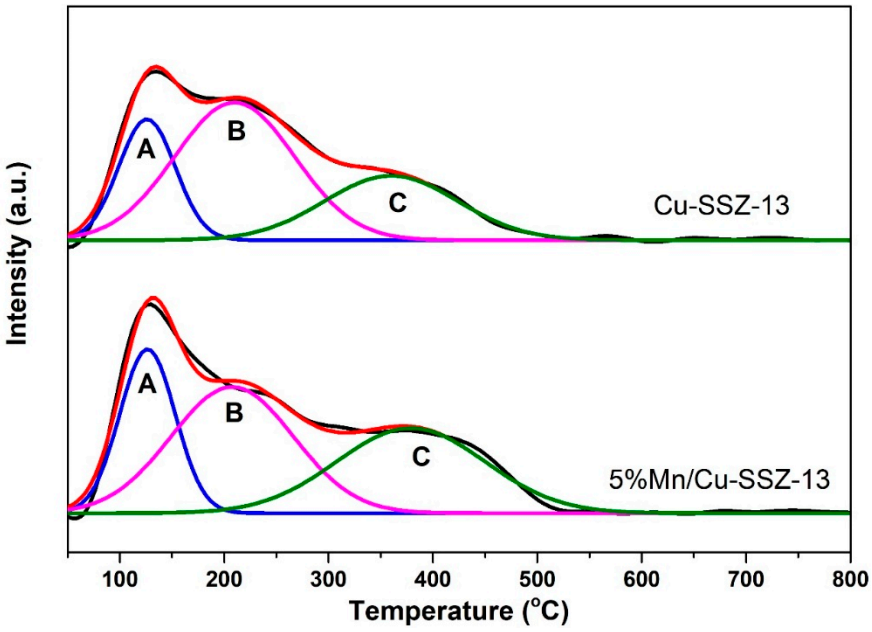

Figure 5. NH_3-TPD profiles of Cu-SSZ-13 and 5% Mn/Cu-SSZ-13.

2.3. Investigation of Reaction Process

To further investigate the NH_3-SCR mechanism over Cu-SSZ-13 and 5% Mn/Cu-SSZ-13, a series of in situ DRIFTS experiments were carried out. The reaction between preabsorbed NH_3 and gaseous NO + O_2 over the catalysts was investigated first, and the results are presented in Figure 6. The peaks around 3400–3200 cm^{-1} and 1456 cm^{-1} were assigned to the stretching and bending vibrations of N-H bonds in NH^{4+} absorbed on Brønsted acid sites [16,49–51]. As the reaction progressed, the peak around 1456 cm^{-1} first increased and then decreased. The formation of nitrate species resulted in an increase in the peak area around 1456 cm^{-1}, and these species were then consumed at 60 min [49]. The peaks at 3183 cm^{-1} were assigned to the stretching vibration of NH_3 absorbed on Cu^{2+}. Meanwhile, the peaks at 1619 cm^{-1} and 1255 cm^{-1} were attributed to the asymmetric and symmetric vibrations of NH_3 absorbed on Lewis acid sites [49,51]. The peak at 1255 cm^{-1} kept decreasing after the injection of NO and O_2; however, the peak around 1619 cm^{-1} first decreased and then increased. This phenomenon indicated that the peak around 1619 cm^{-1} was overlapped by peaks from other species. In other reports, the peaks around 1619 cm^{-1} were assigned to nitrate species on Cu^{2+} ions and NH_3 simultaneously absorbed on Lewis acid sites [52,53]. Therefore, in this study, the peak around 1619 cm^{-1} at 60 min was attributed to nitrate species adsorbed on Cu^{2+}. Meanwhile, the peak at 1575 cm^{-1} was also assigned to nitrate species, and nitrate species dominated after NO and O_2 were injected after 60 min [52,53]. The negative peaks at 944 cm^{-1} and 906 cm^{-1} were assigned to the T-O-T vibration disturbed by $Cu(OH)^+$ and Cu^{2+} species, respectively [16,33,54]. These two peaks' tendency can be observed for the peak at 1255 cm^{-1}, and almost all NH_3 species absorbed on Cu^{2+} species were consumed at 60 min.

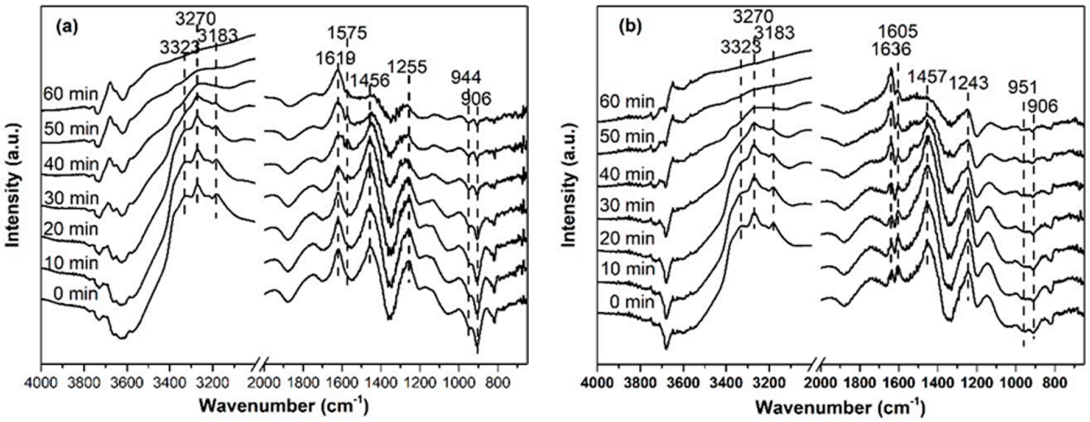

Figure 6. In situ DRIFTS spectra of (**a**) Cu-SSZ-13 and (**b**) 5% Mn/Cu-SSZ-13. Catalysts were exposed to 1000 ppm NH_3/N_2 until saturated and then purged by N_2 to remove weakly absorbed NH_3. 1000 ppm NO/N_2 and 5% O_2 were injected starting at 0 min.

The in situ DRIFTS spectra of 5% Mn/Cu-SSZ-13 are presented in Figure 6b. The characteristic peaks of NH_4^+ species on the Brønsted acid sites of 5% Mn/Cu-SSZ-13 around 3400–3200 cm^{-1} and 1457 cm^{-1} followed the same tendency as observed in Cu-SSZ-13. This indicates that nitrate species are also critical intermediates in the NH_3-SCR process over 5% Mn/Cu-SSZ-13. Apart from Cu^{2+} species, Mn^{n+} species also acted as Lewis acid sites in 5% Mn/Cu-SSZ-13. Unlike the spectra of Cu-SSZ-13, two separate peaks at 1636 cm^{-1} and 1605 cm^{-1} assigned to the NH_3 absorbed on Cu^{2+} and Mn ions were observed for 5% Mn/Cu-SSZ-13, respectively [25,26,39,49,51]. The presence of Mn ions influenced the Cu^{2+} species; therefore, the peak for NH_3 absorbed on Cu^{2+} moved to higher wavenumbers when compared with the spectrum of Cu-SSZ-13. Meanwhile, the intensity of negative peaks related to Cu species (around 951 cm^{-1} and 906 cm^{-1}) decreased when compared with Cu-SSZ-13, which also indicated that Cu^{2+} species were influenced by the addition of Mn. Furthermore, the peak at 1243 cm^{-1} was assigned to the symmetric vibration of NH_3 absorbed on Lewis acid sites, as indicated in Figure 6a [51]. As the reaction progressed, there was a decrease in the peak areas at 1243 cm^{-1},

951 cm^{-1} and 906 cm^{-1}, indicating that NH_3 absorbed on Lewis acid sites was continuously consumed after NO and O_2 were introduced. However, the peak area at 1636 cm^{-1} increased with the passage of time. This indicated that the peak corresponding to nitrate species overlapped the peak for NH_3 absorbed on Lewis acid sites at 1636 cm^{-1}, and abundant nitrate species accumulated after NO and O_2 were added for 60 min.

To sum up, similar NH_3-SCR mechanisms were observed for Cu-SSZ-13 and 5% Mn/Cu-SSZ-13. With the injection of NO and O_2, nitrate species formed and acted as an important intermediate, indicating that the L-H mechanism took place for both catalysts. Meanwhile, NH_3 absorbed on Lewis acid sites was continuously consumed after NO and O_2 were introduced, which meant that the E-R mechanism also played a role. As a result, the L-H and E-R mechanisms coexisted in the NH_3-SCR process over Cu-SSZ-13 and 5% Mn/Cu-SSZ-13.

The reaction between nitrate species and NH_3 was studied. First, catalysts were exposed to NO and O_2 for 1 h until saturated, and NH_3 was introduced from 0 min after purging by N_2 for 1 h. As can be seen in Figure 7a, the peaks between 1650–1500 cm^{-1} were assigned to Cu-NO_3^- species [49,55,56]. After NH_3 was introduced, the intensity of these peaks decreased, indicating that nitrate species were consumed by NH_3, which further proved that the L-H mechanism existed during NH_3-SCR for the catalysts. The peaks around 3400–3200 cm^{-1} and 1457 cm^{-1} were attributed to NH_4^+ species on Brønsted acid sites and began to emerge at 6 min [16,49–51]. Meanwhile, the negative peaks at 951 cm^{-1} and 906 cm^{-1}, which were respectively assigned to $Cu(OH)^+$ and Cu^{2+} species, emerged at 4 min [16,33,54]. Furthermore, new peaks at 1622 cm^{-1} and 1257 cm^{-1} emerged at 4 min, and they were assigned to the asymmetric and symmetric vibrations of NH_3 absorbed on Lewis acid sites [49,51]. A new peak emerging at 1622 cm^{-1} overlapped the peak resulting from nitrate species, but the reaction process could be investigated by observing the peak at 1575 cm^{-1}. After around 16 min, the peak at 1575 cm^{-1} disappeared, indicating that the absorbed nitrate species were consumed. This process was faster than the reaction between absorbed NH_3 and NO + O_2, as presented in Figure 7. This indicated that, compared with the E-R mechanism, the L-H mechanism proceeded more rapidly for the Cu-SSZ-13 used in this study.

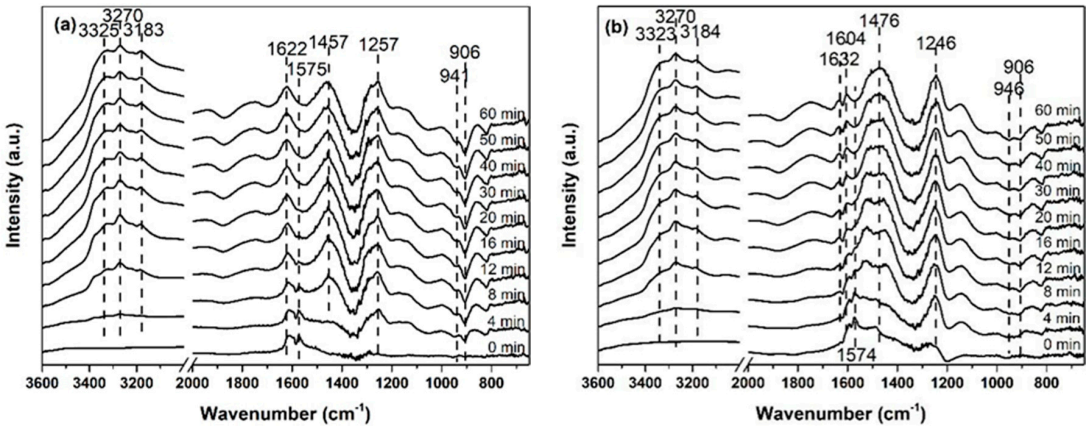

Figure 7. In situ DRIFTS spectra of (**a**) Cu-SSZ-13 and (**b**) 5% Mn/Cu-SSZ-13. Catalysts were exposed to 1000 ppm NO/N_2 and 5% O_2 until saturated and then purged by N_2 to remove weakly absorbed NO and O_2. 1000 ppm NH_3/N_2 was introduced at 0 min.

A similar process was observed for 5% Mn/Cu-SSZ-13, as presented in Figure 7b. The peaks around 1650–1500 cm^{-1} were assigned to Cu-NO_3^- species [49,55,56]. Compared with Cu-SSZ-13, more Cu-NO_3^- species emerged in the spectrum of 5% Mn/Cu-SSZ-13. Meanwhile, the peak at 1574 cm^{-1} could hardly be seen after 8 min when compared to 16 min in Cu-SSZ-13, which meant that Cu-NO_3^- species were consumed more rapidly with 5% Mn/Cu-SSZ-13. Furthermore, the peaks around 1300 cm^{-1} and 1200 cm^{-1} were assigned to bidentate nitrate species in 5% Mn/Cu-SSZ-13, and these

species can hardly be seen in Cu-SSZ-13 [55,57]. New peaks at 1632 cm^{-1}, 1604 cm^{-1} and 1246 cm^{-1} assigned to NH_3 absorbed on Lewis acid sites emerged starting at 2 min [49,51]. Negative peaks at 946 and 906 representing $Cu(OH)^+$ and Cu^{2+} species also appeared at 2 min [16,33,54]. Furthermore, peaks around 3400–3200 cm^{-1} and 1476 cm^{-1}, which represented NH_4^+ species absorbed on Brønsted acid sites, also emerged at 4 min [16,49–51].

In conclusion, after being exposed to NO and O_2, 5% Mn/Cu-SSZ-13 possessed more nitrate species than Cu-SSZ-13, and these species were consumed more rapidly in 5% Mn/Cu-SSZ-13. As we discussed above, the L-H mechanism played an important role in the NH_3-SCR process of our catalysts, and nitrate species were critical intermediates in the L-H mechanism process. The NH_3-SCR process over Cu-SSZ-13 can be regarded as the redox cycle of Cu^+/Cu^{2+}. Cu^{2+} ions were reduced by NO and NH_3, forming N_2 and H_2O, which consisted of the reduction half cycle. In the oxidation half cycle, two Cu^+ ions migrated into one cage to activate O_2 and NO, forming nitrate species, and this was the rate-determining step of the whole process [9,12,41,54]. However, with the addition of Mn, the interaction between Mn and Cu facilitated the redox ability of catalysts; meanwhile, MnO_x species are also excellent catalysts for NO oxidation [39], so that nitrates formed more easily in 5% Mn/Cu-SSZ-13 and the former rate-determining step was avoided. As a result, 5% Mn/Cu-SSZ-13 exhibited a better NH_3-SCR performance than Cu-SSZ-13.

2.4. The Stability of 5% Mn/Cu-SSZ-13

To investigate the stability of the catalysts, an NH_3-SCR catalytic activity durability test was carried out, and the results are presented in Figure 8. 5% Mn/Cu-SSZ-13 was chosen as the testing sample due to it having performed the best among all catalysts; meanwhile, the temperature was set at 135 °C when a high NO_x conversion could be obtained and it was not over 100%. After being tested for 24 h, about 90% of NO_x conversion could still be obtained, and no obvious decrease of the catalytic activity was observed. Furthermore, an XRD experiment was also conducted on the fresh 5% Mn/Cu-SSZ-13 catalyst, 5% Mn/Cu-SSZ-13 catalyst tested for NH_3-SCR at 135 °C for 24 h and 5% Mn/Cu-SSZ-13 catalyst tested for NH_3-SCR in the whole temperature range. As can be seen in Figure S7, no obvious decrease of the crystallinity was observed in the catalysts that were either tested at 135 °C for 24 h or tested across the whole temperature range. Durability is of great importance in order for NH_3-SCR catalysts to be utilized in diesel vehicles, and the results indicated that the 5% Mn/Cu-SSZ-13 catalyst possessed excellent stability as well as a bright future in practical applications.

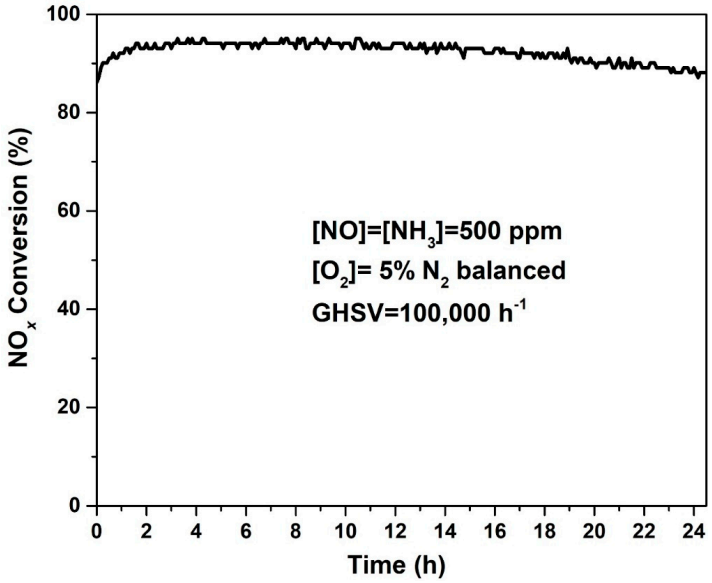

Figure 8. NH_3-SCR activity test of 5% Mn/Cu-SSZ-13 at 135 °C for 24 h.

3. Materials and Methods

3.1. Catalyst Preparation

Cu-SSZ-13 catalysts with 4.6 wt% Cu and an Si/Al ratio of 4.8 were prepared by an in situ synthesis method described previously [14,15,58]. To obtain Mn/Cu-SSZ-13 catalysts with a varying Mn content, Cu-SSZ-13 was impregnated with manganese acetate ($C_4H_6MnO_4{\cdot}4H_2O$) (SINOPHARM, Beijing, China) solutions of different concentrations. First, 5 g of Cu-SSZ-13 catalyst powder was dispersed in 500 mL deionized water and stirred for 1 h. Then, different amounts of manganese acetate with the equivalent Mn weight of 0.15 g, 0.25 g, 0.35 g, 0.5 g and 0.7 g were added into the solution and stirred for 2 h. The obtained solution was evaporated to dryness by a rotary evaporator at 50 °C, and the powder was placed overnight in an oven at 80 °C. Finally, all the Cu-SSZ-13 powders with and without Mn addition were calcined at 600 °C for 6 h with a ramp rate of 10 °C/min. The obtained catalysts were denoted as Cu-SSZ-13, 3% Mn/Cu-SSZ-13, 5% Mn/Cu-SSZ-13, 7% Mn/Cu-SSZ-13, 10% Mn/Cu-SSZ-13 and 14% Mn/Cu-SSZ-13, respectively.

3.2. Catalyst Characterization

SEM (scanning electron microscopy) (HITACHI, Beijing, China) was utilized to observe the morphology of the catalysts. EDX (Energy Dispersive X-Ray Spectroscopy) (HITACHI, Beijing, China) was used to detect the atoms on the surface of the catalysts. XRD (X-ray diffraction) was carried out to analyze the crystal structure of the catalysts, using a Brucker D8 Advance diffractometer (Brucker, Beijing, China) with Cu Kα (λ = 0.15406 nm). The scan range was from 5°–90°, with step size of 0.02°. N_2 adsorption-desorption was carried out to compare the surface areas and pore volumes of the catalysts before and after Mn addition. The surface area of the catalysts was calculated by the multipore BET method, and the micropore volume was calculated by the t-plot method.

H_2-TPR was carried out to evaluate the redox ability of the catalysts, and the experiment was conducted on a chemisorption analyzer (Micromeritics AutoChem 2920, Beijing, China). First, the catalysts were pretreated under 20% O_2/N_2 at 500 °C for 1 h. After cooling down to room temperature, H_2/Ar was introduced. After the baseline was stable, the temperature was raised to 800 °C with a ramp rate of 10 °C/min. XPS (X-ray photoelectron spectroscopy) (Thermo, Beijing, China) was utilized to detect the valance state of atoms in the catalysts. NH_3-TPD (temperature programmed desorption of NH_3) (Thermo, Beijing, China) was conducted to characterize the acidity of the catalysts. 100 mg of catalyst was placed into a quartz tube sealed at both ends with quartz wool. Catalysts were pretreated at 500 °C under 20% O_2/N_2 for 1 h. After cooling to 50 °C, 500 ppm NH_3/N_2 was introduced until the catalysts were saturated with NH_3, after which the catalysts were purged by N_2 until all the unabsorbed NH_3 was removed. Finally, with a total flow of N_2 of 250 mL/min, the catalysts were heated from 50 °C to 800 °C with a ramp rate of 10 °C/min. The composition of the outlet gas was analyzed by a Nicolet IS 10 infrared spectrometer (Thermo, Beijing, China).

In situ DRIFTS (diffuse reflectance infrared Fourier transform spectroscopy) was used to investigate the reaction mechanism over different catalysts, and the experiments were carried out on a Nicolet IS50 spectrometer (Thermo, Beijing, China) with an MCT/A detector. All catalysts were pretreated at 500 °C for 30 min with 20% O_2/N_2 before the reaction. The whole reaction process was conducted at 150 °C with a total gas flow of 100 mL/min, and the concentrations of NO, NH_3 and O_2 were 1000 ppm, 1000 ppm and 5%, respectively. The first series of experiments were carried out to investigate the reaction between adsorbed NH_3 and gaseous NO + O_2. Catalysts were exposed to NH_3 until saturated and then purged by N_2 to eliminate surplus NH_3. Then, NO and O_2 were introduced, and the spectra were collected. In the second series of experiments, the reaction between adsorbed NO + O_2 and gaseous NH_3 was investigated. NO and O_2 were introduced to the catalysts until saturated, after which the unabsorbed gas was purged by N_2. Finally, NH_3 was introduced, and the spectra were recorded.

3.3. Catalytic Tests

NH_3-SCR tests were carried out in a fixed bed reactor (WeiYe, Beijing, China), with the catalysts loaded in quartz tubes sealed by quartz wool. All the catalysts were sieved to a 40–60 mesh before the NH_3-SCR tests. The total gas flow was 250 mL/min with the gas composition: [NO] = [NH_3] = 500 ppm, [O_2] = 5%, N_2 balance, and GHSV = 100,000 h^{-1}. The outlet gas was detected by a Nicolet IS 10 infrared spectrometer, and the NO_x conversion was calculated by the following equation:

$$NO_x\ conversion\ = \left(1 - \frac{[NO_x]_{out}}{[NO_x]_{in}}\right) \times 100\%\ (NO_x\ =\ NO\ +\ NO_2)$$

4. Conclusions

In this study, it was found that impregnation with an appropriate amount of Mn could efficiently improve the low-temperature catalytic activity of in situ synthesized Cu-SSZ-13. The promotion effect of Mn on Cu-SSZ-13 was thoroughly investigated from the aspects of the structural framework, redox ability, acid sites and reaction mechanism. It was observed that MnO_x species tended to be located in the pores of Cu-SSZ-13 in a highly dispersed form. Meanwhile, the addition of Mn markedly facilitated the redox ability of Cu-SSZ-13. The improvement of the redox ability promoted the formation of nitrate species, which were critical intermediates in the NH_3-SCR process. As a result, the low-temperature catalytic performance was greatly improved in Mn-impregnated Cu-SSZ-13 catalysts.

Supplementary Materials: The following are available online at http://www.mdpi.com/2073-4344/10/12/1375/s1, Figure S1: Concentration of N_2O produced by the prepared catalysts under NH_3-SCR conditions. Figure S2: SEM images of prepared catalysts. (a) Cu-SSZ-13, (b) 3% Mn/Cu-SSZ-13, (c) 5% Mn/Cu-SSZ-13, (d) 7% Mn/Cu-SSZ-13, (e) 10% Mn/Cu-SSZ-13, (f) 14% Mn/Cu-SSZ-13. Figure S3: EDX results of catalysts. (a) Cu-SSZ-13, (b) 5% Mn/Cu-SSZ-13. Figure S4: XRD patterns of Cu-SSZ-13 catalysts with and without Mn impregnation. Figure S5: XPS spectra of catalysts. (a) Cu 2p spectra of Cu-SSZ-13 and 5% Mn/Cu-SSZ-13, (b) Mn 2p spectra of 5% Mn/Cu-SSZ-13. Figure S6: Integrated NH_3 desorption amounts per 1 g of catalyst, calculated from NH_3-TPD results. Figure S7. XRD patterns of 5% Mn/Cu-SSZ-13 catalysts before and after being used.

Author Contributions: H.H., Y.S. and Y.Z. designed the experiments; J.D. and J.W. performed the experiments, analyzed the data and wrote the manuscript; X.S. and H.H. checked and corrected the manuscript. All authors have read and agreed to the published version of the manuscript.

Funding: We wish to express our appreciation for funding from the National Natural Science Foundation of China (grant number: 21637005, 21906172). We also appreciate the funding and support received from Sinopec: Technology Development Contract (contract number: 319002).

Conflicts of Interest: The authors declare no conflict of interest.

References

1. Tan, Y.; Henderick, P.; Yoon, S.; Herner, J.; Montes, T.; Boriboonsomsin, K.; Johnson, K.; Scora, G.; Sandez, D.; Durbin, T.D. On-Board Sensor-Based NO_x Emissions from Heavy-Duty Diesel Vehicles. *Environ. Sci. Technol.* **2019**, *53*, 5504–5511. [CrossRef] [PubMed]
2. Walters, W.W.; Goodwin, S.R.; Michalski, G. Nitrogen stable isotope composition (delta^{15}N) of vehicle-emitted NO_x. *Environ. Sci. Technol.* **2015**, *49*, 2278–2285. [CrossRef] [PubMed]
3. Yang, L.; Franco, V.; Mock, P.; Kolke, R.; Zhang, S.; Wu, Y.; German, J. Experimental Assessment of NO_x Emissions from 73 Euro 6 Diesel Passenger Cars. *Environ. Sci. Technol.* **2015**, *49*, 14409–14415. [CrossRef] [PubMed]
4. Wang, P.; Chen, S.; Gao, S.; Zhang, J.; Wang, H.; Wu, Z. Niobium oxide confined by ceria nanotubes as a novel SCR catalyst with excellent resistance to potassium, phosphorus, and lead. *Appl. Catal. B Environ.* **2018**, *231*, 299–309. [CrossRef]
5. Cai, S.; Zhang, D.; Zhang, L.; Huang, L.; Li, H.; Gao, R.; Shi, L.; Zhang, J. Comparative study of 3D ordered macroporous $Ce_{0.75}Zr_{0.2}M_{0.05}O_{2-\delta}$ (M = Fe, Cu, Mn, Co) for selective catalytic reduction of NO with NH_3. *Catal. Sci. Technol.* **2014**, *4*, 93–101. [CrossRef]
6. Li, P.; Xin, Y.; Li, Q.; Wang, Z.; Zhang, Z.; Zheng, L. Ce-Ti amorphous oxides for selective catalytic reduction of NO with NH_3: Confirmation of Ce-O-Ti active sites. *Environ. Sci. Technol.* **2012**, *46*, 9600–9605. [CrossRef]

7. Chen, Y.; Li, C.; Chen, J.; Tang, X. Self-Prevention of Well-Defined-Facet Fe_2O_3/MoO_3 against Deposition of Ammonium Bisulfate in Low-Temperature NH_3-SCR. *Environ. Sci. Technol.* **2018**, *52*, 11796–11802. [CrossRef]
8. Han, S.; Ye, Q.; Cheng, S.; Kang, T.; Dai, H. Effect of the hydrothermal aging temperature and Cu/Al ratio on the hydrothermal stability of CuSSZ-13 catalysts for NH_3-SCR. *Catal. Sci. Technol.* **2017**, *7*, 703–717. [CrossRef]
9. Gao, F.; Peden, C.H. Recent Progress in Atomic-Level Understanding of Cu/SSZ-13 Selective Catalytic Reduction Catalysts. *Catalysts* **2018**, *8*, 140. [CrossRef]
10. Kwak, J.H.; Tonkyn, R.G.; Kim, D.H.; Szanyi, J.; Peden, C.H.F. Excellent activity and selectivity of Cu-SSZ-13 in the selective catalytic reduction of NO_x with NH_3. *J. Catal.* **2010**, *275*, 187–190. [CrossRef]
11. Kwak, J.H.; Tran, D.; Burton, S.D.; Szanyi, J.; Lee, J.H.; Peden, C.H.F. Effects of hydrothermal aging on NH_3-SCR reaction over Cu/zeolites. *J. Catal.* **2012**, *287*, 203–209. [CrossRef]
12. Paolucci, C.; Khurana, I.; Parekh, A.A.; Li, S.; Shih, A.J.; Li, H.; Di Iorio, J.R.; Albarracin-Caballero, J.D.; Yezerets, A.; Miller, J.T.; et al. Dynamic multinuclear sites formed by mobilized copper ions in NO_x selective catalytic reduction. *Science* **2017**, *357*, 898–903. [CrossRef] [PubMed]
13. Gao, F.; Kwak, J.; Szanyi, J.; Peden, C.F. Current Understanding of Cu-Exchanged Chabazite Molecular Sieves for Use as Commercial Diesel Engine DeNO_x Catalysts. *Top. Catal.* **2013**, *56*, 1441–1459. [CrossRef]
14. Ren, L.; Zhu, L.; Yang, C.; Chen, Y.; Sun, Q.; Zhang, H.; Li, C.; Nawaz, F.; Meng, X.; Xiao, F.S. Designed copper-amine complex as an efficient template for one-pot synthesis of Cu-SSZ-13 zeolite with excellent activity for selective catalytic reduction of NO_x by NH_3. *Chem. Commun.* **2011**, *47*, 9789–9791. [CrossRef] [PubMed]
15. Ren, L.; Zhang, Y.; Zeng, S.; Zhu, L.; Sun, Q.; Zhang, H.; Yang, C.; Meng, X.; Yang, X.; Xiao, F.-S. Design and Synthesis of a Catalytically Active Cu-SSZ-13 Zeolite from a Copper-Amine Complex Template. *Chin. J. Catal.* **2012**, *33*, 92–105. [CrossRef]
16. Shan, Y.; Du, J.; Yu, Y.; Shan, W.; Shi, X.; He, H. Precise control of post-treatment significantly increases hydrothermal stability of in-situ synthesized cu-zeolites for NH_3-SCR reaction. *Appl. Catal. B Environ.* **2020**, *266*. [CrossRef]
17. Xie, L.; Liu, F.; Shi, X.; Xiao, F.-S.; He, H. Effects of post-treatment method and Na co-cation on the hydrothermal stability of Cu–SSZ-13 catalyst for the selective catalytic reduction of NO_x with NH_3. *Appl. Catal. B Environ.* **2015**, *179*, 206–212. [CrossRef]
18. Wang, D.; Gao, F.; Peden, C.H.F.; Li, J.; Kamasamudram, K.; Epling, W.S. Selective Catalytic Reduction of NO_x with NH_3 over a Cu-SSZ-13 Catalyst Prepared by a Solid-State Ion-Exchange Method. *ChemCatChem* **2014**, *6*, 1579–1583. [CrossRef]
19. Kim, J.; Cho, S.J.; Kim, D.H. Facile Synthesis of KFI-type Zeolite and Its Application to Selective Catalytic Reduction of NO_x with NH_3. *ACS Catal.* **2017**, *7*, 6070–6081. [CrossRef]
20. Hammershøi, P.S.; Negri, C.; Berlier, G.; Bordiga, S.; Beato, P.; Janssens, T.V.W. Temperature-programmed reduction with NO as a characterization of active Cu in Cu-CHA catalysts for NH_3-SCR. *Catal. Sci. Technol.* **2019**, *9*, 2608–2619. [CrossRef]
21. Liu, Z.; Yi, Y.; Zhang, S.; Zhu, T.; Zhu, J.; Wang, J. Selective catalytic reduction of NO_x with NH_3 over Mn-Ce mixed oxide catalyst at low temperatures. *Catal. Today* **2013**, *216*, 76–81. [CrossRef]
22. Meng, D.; Zhan, W.; Guo, Y.; Guo, Y.; Wang, L.; Lu, G. A Highly Effective Catalyst of Sm-MnO_x for the NH_3-SCR of NO_x at Low Temperature: Promotional Role of Sm and Its Catalytic Performance. *ACS Catal.* **2015**, *5*, 5973–5983. [CrossRef]
23. Kang, M.; Park, E.D.; Kim, J.M.; Yie, J.E. Cu–Mn mixed oxides for low temperature NO reduction with NH_3. *Catal. Today* **2006**, *111*, 236–241. [CrossRef]
24. Zuo, J.; Chen, Z.; Wang, F.; Yu, Y.; Wang, L.; Li, X. Low-Temperature Selective Catalytic Reduction of NO_x with NH_3 over Novel Mn–Zr Mixed Oxide Catalysts. *Ind. Eng. Chem. Res.* **2014**, *53*, 2647–2655. [CrossRef]
25. Wu, S.; Zhang, L.; Wang, X.; Zou, W.; Cao, Y.; Sun, J.; Tang, C.; Gao, F.; Deng, Y.; Dong, L. Synthesis, characterization and catalytic performance of Fe$MnTiO_x$ mixed oxides catalyst prepared by a CTAB-assisted process for mid-low temperature NH_3-SCR. *Appl. Catal. A Gen.* **2015**, *505*, 235–242. [CrossRef]
26. Yan, Q.; Chen, S.; Zhang, C.; Wang, Q.; Louis, B. Synthesis and catalytic performance of $Cu_1Mn_{0.5}Ti_{0.5}O_x$ mixed oxide as low-temperature NH_3 -SCR catalyst with enhanced SO_2 resistance. *Appl. Catal. B Environ.* **2018**, *238*, 236–247. [CrossRef]

27. Tang, X.; Wang, C.; Gao, F.; Ma, Y.; Yi, H.; Zhao, S.; Zhou, Y. Effect of hierarchical element doping on the low-temperature activity of manganese-based catalysts for NH_3-SCR. *J. Environ. Chem. Eng.* **2020**, *8*, 104399–104408. [CrossRef]
28. Qi, G.; Yang, R.T.; Chang, R. MnO_x-CeO_2 mixed oxides prepared by co-precipitation for selective catalytic reduction of NO with NH_3 at low temperatures. *Appl. Catal. B Environ.* **2004**, *51*, 93–106. [CrossRef]
29. Ye, Y.; Shen, F.; Wang, H.; Chen, R. SSZ-13-supported manganese oxide catalysts for low temperature selective catalytic reduction of NO_x by NH3. *J. Chem. Sci.* **2017**, *129*, 765–774. [CrossRef]
30. Kim, Y.J.; Kwon, H.J.; Heo, I.; Nam, I.-S.; Cho, B.K.; Choung, J.W.; Cha, M.-S.; Yeo, G.K. Mn–Fe/ZSM5 as a low-temperature SCR catalyst to remove NO_x from diesel engine exhaust. *Appl. Catal. B Environ.* **2012**, *126*, 9–21. [CrossRef]
31. Yao, W.; Gang-gang, L.; Shao-qing, Z.; Xin-yan, Z.; Xin, Z.; Zheng-ping, H. Promoting effect of Ce and Mn addition on Cu-SSZ-39 zeolites for NH3-SCR reaction: Activity, hydrothermal stability, and mechanism study. *Chem. Eng. J.* **2020**, *393*. [CrossRef]
32. Song, C.; Zhang, L.; Li, Z.; Luac, Y.; Li, K. Co-Exchange of Mn: A Simple Method to Improve Both the Hydrothermal Stability and Activity of Cu–SSZ-13 NH3–SCR Catalysts. *Catalysts* **2019**, *9*, 455. [CrossRef]
33. Shan, Y.; Shan, W.; Shi, X.; Du, J.; Yu, Y.; He, H. A comparative study of the activity and hydrothermal stability of Al-rich Cu-SSZ-39 and Cu-SSZ-13. *Appl. Catal. B Environ.* **2020**, *264*, 118511. [CrossRef]
34. Shan, Y.; Sun, Y.; Du, J.; Zhang, Y.; He, H.; Yu, Y.; Shan, W.; He, H. Hydrothermal aging alleviates the inhibition effects of NO2 on Cu-SSZ-13 for NH3-SCR. *Appl. Catal. B Environ.* **2020**, *275*, 119105. [CrossRef]
35. Kwak, J.H.; Zhu, H.; Lee, J.H.; Peden, C.H.F.; Szanyi, J. Two different cationic positions in Cu-SSZ-13? *Chem. Commun.* **2012**, *48*, 4758–4760. [CrossRef]
36. Kim, Y.J.; Lee, J.K.; Min, K.M.; Hong, S.B.; Nam, I.-S.; Cho, B.K. Hydrothermal stability of CuSSZ13 for reducing NO_x by NH3. *J. Catal.* **2014**, *311*, 447–457. [CrossRef]
37. Wang, Y.; Shi, X.; Shan, Y.; Du, J.; Liu, K.; He, H. Hydrothermal Stability Enhancement of Al-Rich Cu-SSZ-13 for NH3 Selective Catalytic Reduction Reaction by Ion Exchange with Cerium and Samarium. *Ind. Eng. Chem. Res.* **2020**, *59*, 6416–6423. [CrossRef]
38. Du, J.; Qu, Z.; Dong, C.; Song, L.; Qin, Y.; Huang, N. Low-temperature abatement of toluene over Mn-Ce oxides catalysts synthesized by a modified hydrothermal approach. *Appl. Surf. Sci.* **2018**, *433*, 1025–1035. [CrossRef]
39. Sun, P.; Guo, R.-T.; Liu, S.-M.; Wang, S.-X.; Pan, W.-G.; Li, M.-Y. The enhanced performance of MnO_x catalyst for NH3-SCR reaction by the modification with Eu. *Appl. Catal. A Gen.* **2017**, *531*, 129–138. [CrossRef]
40. Deng, H.; Kang, S.; Ma, J.; Wang, L.; Zhang, C.; He, H. Role of Structural Defects in MnO_x Promoted by Ag Doping in the Catalytic Combustion of Volatile Organic Compounds and Ambient Decomposition of O3. *Environ. Sci. Technol.* **2019**, *53*, 10871–10879. [CrossRef]
41. Li, X.; Ma, J.; He, H. Tuning the Chemical State of Silver on Ag–Mn Catalysts to Enhance the Ozone Decomposition Performance. *Environ. Sci. Technol.* **2020**, *54*, 11566–11575. [CrossRef] [PubMed]
42. Gao, F.; Mei, D.; Wang, Y.; Szanyi, J.; Peden, C.H.F. Selective Catalytic Reduction over Cu/SSZ-13: Linking Homo- and Heterogeneous Catalysis. *J. Am. Chem. Soc.* **2017**, *139*, 4935–4942. [CrossRef] [PubMed]
43. Yu, T.; Xu, M.; Huang, Y.; Wang, J.; Wang, J.; Lv, L.; Qi, G.; Li, W.; Shen, M. Insight of platinum poisoning Cu/SAPO-34 during NH3-SCR and its promotion on catalysts regeneration after hydrothermal treatment. *Appl. Catal. B Environ.* **2017**, *204*, 525–536. [CrossRef]
44. Wang, J.; Yu, T.; Wang, X.; Qi, G.; Xue, J.; Shen, M.; Li, W. The influence of silicon on the catalytic properties of Cu/SAPO-34 for NO_x reduction by ammonia-SCR. *Appl. Catal. B Environ.* **2012**, *127*, 137–147. [CrossRef]
45. Liu, X.; Xiaodong, W.; Weng, D.; Si, Z.; Ran, R. Evolution of copper species on Cu/SAPO-34 SCR catalysts upon hydrothermal aging. *Catal. Today* **2017**, *281*, 596–604. [CrossRef]
46. Chen, X.; Wang, P.; Fang, P.; Ren, T.; Liu, Y.; Cen, C.; Wang, H.; Wu, Z. Tuning the property of Mn-Ce composite oxides by titanate nanotubes to improve the activity, selectivity and SO2/H2O tolerance in middle temperature NH3-SCR reaction. *Fuel Process. Technol.* **2017**, *167*, 221–228. [CrossRef]
47. Tian, W.; Yang, H.; Fan, X.; Zhang, X. Catalytic reduction of NO_x with NH3 over different-shaped MnO2 at low temperature. *J. Hazard. Mater.* **2011**, *188*, 105–109. [CrossRef] [PubMed]
48. Yang, G.; Zhao, H.; Luo, X.; Shi, K.; Wang, W.; Chen, Q.; Fan, H.; Wu, T. Promotion effect and mechanism of the addition of Mo on the enhanced low temperature SCR of NO_x by NH3 over MnO_x/γ-Al2O3 catalysts. *Appl. Catal. B Environ.* **2019**, *245*, 743–752. [CrossRef]

49. Xie, L.; Liu, F.; Liu, K.; Shi, X.; He, H. Inhibitory effect of NO2 on the selective catalytic reduction of NO_x with NH3 over one-pot-synthesized Cu–SSZ-13 catalyst. *Catal. Sci. Technol.* **2014**, *4*, 1104–1110. [CrossRef]
50. Shi, X.; Liu, F.; Xie, L.; Shan, W.; He, H. NH3-SCR Performance of Fresh and Hydrothermally Aged Fe-ZSM-5 in Standard and Fast Selective Catalytic Reduction Reactions. *Environ. Sci. Technol.* **2013**, *47*, 3293–3298. [CrossRef] [PubMed]
51. Lezcano-Gonzalez, I.; Deka, U.; Arstad, B.; Deyne, A.V.Y.-D.; Hemelsoet, K.; Waroquier, M.; Van Speybroeck, V.; Weckhuysen, B.M.; Beale, A.M. Determining the storage, availability and reactivity of NH3within Cu-Chabazite-based Ammonia Selective Catalytic Reduction systems. *Phys. Chem. Chem. Phys.* **2014**, *16*, 1639–1650. [CrossRef] [PubMed]
52. Kubota, H.; Liu, C.; Toyao, T.; Maeno, Z.; Ogura, M.; Nakazawa, N.; Inagaki, S.; Kubota, Y.; Shimizu, K.-I. Formation and Reactions of NH4NO3 during Transient and Steady-State NH3-SCR of NO_x over H-AFX Zeolites: Spectroscopic and Theoretical Studies. *ACS Catal.* **2020**, *10*, 2334–2344. [CrossRef]
53. Ruggeri, M.P.; Nova, I.; Tronconi, E.; Pihl, J.A.; Toops, T.J.; Partridge, W.P. In-situ DRIFTS measurements for the mechanistic study of NO oxidation over a commercial Cu-CHA catalyst. *Appl. Catal. B Environ.* **2015**, 181–192. [CrossRef]
54. Du, J.; Shi, X.; Shan, Y.; Xu, G.; Sun, Y.; Wang, Y.; Yu, Y.; Shan, W.; He, H. Effects of SO2 on Cu-SSZ-39 catalyst for the selective catalytic reduction of NO_x with NH3. *Catal. Sci. Technol.* **2020**, *10*, 1256–1263. [CrossRef]
55. Zhang, Y.; Peng, Y.; Li, K.; Liu, S.; Chen, J.; Li, J.; Gao, F.; Peden, C.H.F. Using Transient FTIR Spectroscopy to Probe Active Sites and Reaction Intermediates for Selective Catalytic Reduction of NO on Cu/SSZ-13 Catalysts. *ACS Catal.* **2019**, *9*, 6137–6145. [CrossRef]
56. Chen, H.-Y.; Wei, Z.; Kollar, M.; Gao, F.; Wang, Y.; Szanyi, J.; Peden, C.H.F. A comparative study of N2O formation during the selective catalytic reduction of NO_x with NH3 on zeolite supported Cu catalysts. *J. Catal.* **2015**, *329*, 490–498. [CrossRef]
57. Hadjiivanov, K.I. Identification of Neutral and Charged NxOySurface Species by IR Spectroscopy. *Catal. Rev.* **2000**, *42*, 71–144. [CrossRef]
58. Xie, L.; Liu, F.; Ren, L.; Shi, X.; Xiao, F.-S.; He, H. Excellent Performance of One-Pot Synthesized Cu-SSZ-13 Catalyst for the Selective Catalytic Reduction of NO_x with NH3. *Environ. Sci. Technol.* **2013**, *48*, 566–572. [CrossRef]